A comparison of three dual drainage models: Shallow Water vs Local Inertial vs Diffusive Wave

Ricardo Martins [1,3,4,*], Jorge Leandro [2,3,4], Albert S. Chen [5], Slobodan Djordjević [5]

[1] Dept. of Civil and Structural Engineering, Mappin Building, S1 3JD University of Sheffield, Sheffield, UK

[2] Department of Civil, Geo and Environmental Engineering, Chair of Hydrology and River Basin Management, Technical University of Munich, Arcisstrasse 21, 80333 Munich, Germany

[3] MARE - Marine and Environmental Sciences Centre, Department of Civil Engineering, FCT, University of Coimbra, 3004-517 Coimbra, Portugal

[4] IMAR - Institute of Marine Research, Department of Civil Engineering, FCT, University of Coimbra, 3004-517 Coimbra, Portugal

[5] Centre for Water Systems, University of Exeter, North Park Road, Exeter EX4 4QF, United Kingdom

* corresponding author. Email: ricardo.martins@sheffield.ac.uk

Abstract

In this study we compared three overland flow models, a full dynamic model (SWE), a local inertial equations model (GWM), and a diffusive wave model (PDWAVE). The three models are coupled with the same full dynamic sewer network model (SIPSON). We adopted the volume exchange between sewer and overland flow models, and the hydraulic head and discharge rates at the linked manholes to evaluate differences between the models. For that purpose we developed a novel methodology based on RGB scale. The test results of a real case study show a close agreement between coupled models in terms of the extents of flooding, depth and volume exchanged, despite highly complex flows and geometries. The diffusive wave model gives slightly higher maximum flood depths and a slower propagation of the flood front when compared to the other two models. The Local inertial model shows to slight extent higher depths downstream as the wave front is slower than the one in the fully dynamic model. Overall, the simplified overland models can produce comparable results to fully dynamic models with less computational cost.

Introduction

Pluvial floods may cause huge economic damage. Physical scale models require large data extraction instrumentation and installations. Numerical models on the contrary allow a cost efficient solution to simulate floods.

To simulate flood dynamics in urban areas, the drainage network is often divided into two sub-systems: the minor drainage system composed of buried pipes and manholes and the major drainage system that includes watercourses and flow pathways along the surface. An accurate flood model should not only replicate the flow dynamics in the sewer system but also on the surface as well as the interaction between both systems. The flow in the minor system is commonly modelled by one-dimensional (1D) sewer models, while either 1D or two-dimensional (2D) approach (Leandro et al, 2009) can be used to simulate flooding in the major system. 1D/1D models were the first type of urban flood models adopting the dual drainage (DD) concept (Leandro et al, 2011). One of the first proposals for dual drainage was made by Ellis et al. (1982) using SWMM to design Dual Drainage 1D/1D Systems, where the two systems remained separated although they were calibrated as if they worked together. More recently the approach has seen some significant improvements by Prodanovic et al., (1998); Djordjević et al., (1999); Hsu et al, (2002); Nasello and Tucciarelli, (2005); Chen et al, (2007); Leandro et al, (2009); Mahdizadeh et al, (2011, 2012); Seyoum et al, (2012); Borsche and Klar, (2014); Fraga et al,(2015); Chen et al,(2015); Russo et al,(2015); Martins et al,(2016c); Leandro et al, (2016).

Djordjević et al., (1999) proposed an approach to the dual drainage concept to better replicate the urban flood conditions with an integrated sewer and surface hydraulic model. This concept included the use of energy and mass conservation equations to compute the linkage. Nasello and Tucciarelli (2005) applied a similar concept to a 1D/2D model with linkage through weir and orifice equations. The weir and orifice equations are usually calibrated with parameters obtained from experimental studies or using Computational Fluid Dynamics (CFD) simulations that can account for the full complexity of the linkage structure (Lopes et al, 2013; Martins et al, 2014; Leandro et al, 2014b).

Mahdizadeh et al (2011, 2012) introduced a novel model for the shallow water equations (SWEs) where inflowas and outflows are computed using the approach they termed a flux differencing methodology. Abdullah et al (2012) developed a methodology to account for elevated roads and bridges. Seyoum et al (2012) coupled SWMM to a 2D SWE local inertial model. Borsche and Klar (2014) derived a system of ODEs governing the flow in the manholes. Fraga et al (2015) used an experiment in order to validate a 1D/2D coupled model where the rainfall-runoff transformation in urban environments has been validated using a real-scale street section.

Modelling of flow in the major system is usually done with the 2D non-linear SWEs. These equations can be obtained from the Navier-Stokes equations by assuming an incompressible and inviscid fluid, by neglecting the influence of the vertical acceleration and assuming hydrostatic pressure distribution. They are often used to describe a wide range of free surface flows (Chertock et al. 2015). Simplified versions have been developed (Aronica et al, 1998; Chen et al, 2015; Fernández-Pato and García-Navarro, 2016; López-Barrera et al. 2012; Martins et al. 2015; Ponce, 1990) in order to reduce the computational cost whilst maintaining an acceptable level of accuracy. Examples can be seen in the applications of local inertial equations (Aronica et al, 1998; Martins et al, 2016a,b), which neglect the convective acceleration, and diffusive wave equations without inertia (Cea et al., 2010; Chen et al, 2015; Lal, 1998; López-Barrera et al., 2012; Fernández-Pato and García-Navarro, 2016; Wang et al.,

2011) that neglect the convective and local accelerations. The spatial and time discretization used to model surface flows varies in each model.

This paper focuses on the wave propagation of three hydrodynamic models under dual drainage conditions. We compared the models using a novel methodology in a real test case scenario with surcharge from a sewer network. The importance of knowing the limitation of each simplified model in such complex situation is important as the correct assessment of the flood depths is critical for analysis of flood impacts.

Methodology

Surface Models

Three 2D overland flow models were studied: full dynamic model (SWE), Gravity Wave Model (GWM) and Parallel Diffusive Wave Model (PDWAVE). The sequential version of PDWAVE was used in order to be comparable to the other models.

The generic conservation law is presented in Equation (1).

$$\frac{\partial}{\partial t}\boldsymbol{U} + \nabla \cdot \mathcal{F}(\boldsymbol{U}, x, y) - \mathcal{S}(\boldsymbol{U}, x, y) = 0 \tag{1}$$

When using the Manning's friction term to represent the bed friction stress, the third term on the left hand side becomes common to all models and is therefore:

$$\mathcal{S}(\boldsymbol{U}, x, y) = \begin{bmatrix} 0 \\ -\left(ghB_x - ugn^2\sqrt{u^2 + v^2}h^{-1/3}\right) \\ -\left(ghB_y - vgn^2\sqrt{u^2 + v^2}h^{-1/3}\right) \end{bmatrix} \tag{2}$$

In the equations h represents the water depth, u and v the velocity components in the x and y orthogonal direction, respectively, g is the gravitational acceleration, B_x is the bed slope in x direction and B_y is the bed slope in y direction. These equations represent the mass conservation equation and the momentum conservation equations in x and y direction. The first and second left hand terms in Equation (1) are respectively the local acceleration and the convective acceleration.

SWE and GWM

The SWE is given by the following terms in equation (1):

$$\boldsymbol{U} = \begin{bmatrix} h \\ uh \\ vh \end{bmatrix}, \mathcal{F}(\boldsymbol{U}, x, y) = \begin{bmatrix} uh & vh \\ \frac{1}{2}gh^2 & u^2h + uvh \\ v^2h + uvh & \frac{1}{2}gh^2 \end{bmatrix} \tag{3}$$

The GWM is based on the non-linear local inertial equations in conservative form that neglects the convective acceleration terms when compared to the SWE (de Almeida et al., 2012; de Almeida and Bates, 2013). The equations have been used in several flood and river hydraulics applications, for example de Almeida et al., 2012; de Almeida and Bates, 2013; Yamazaki et al. (2013). Its matrix form is:

$$\boldsymbol{U} = \begin{bmatrix} h \\ uh \\ vh \end{bmatrix}, \mathcal{F}(\boldsymbol{U}, x, y) = \begin{bmatrix} uh & vh \\ \frac{1}{2}gh^2 & 0 \\ 0 & \frac{1}{2}gh^2 \end{bmatrix} \tag{4}$$

Both the SWE and the GWM equations are solved using a first order in space and time finite volume method (Martins et al., 2015). The spatial discretisation is based on a 2D node-centred staggered unstructured triangular mesh. The numerical integration of the equations is done with the equations in their integral form and is divided into two steps, the space integral and the time integral. Using Gauss divergence theorem, the area integral is changed to a curve integral that accounts for the fluxes over the boundaries of the cell. The inter-cell fluxes are then evaluated as a 1D Riemann problem between two generic adjacent points (a Roe Approximate Riemann solver) with specific averaged values of the primitive variables derived for the equations. The bed elevation source term is calculated using an upwind scheme, which avoids non-physical oscillations, derived respecting the extended $\mathcal{C}$-property (Castro et al., 2005) by projecting the source term onto the eigenvectors of the flux Jacobian. The source term is linearised and evaluated at the same state as the inter-cell fluxes. Bed friction source term is calculated outside the fluxes with a semi implicit, Runge-Kutta based, point-wise scheme (Liang and Marche, 2009; Song et al., 2011). The Wet-Dry front is treated using Leandro et al. (2014a) approach that avoids localised "negative depths", formulated for each set of equations. Details about these models can be found in Martins et al. (2015). Both models are connected to the 1D storm sewer model SIPSON through flow exchanges at manholes. The time step in the SWE and GWM model is controlled by the CFL condition as defined in Nikolos and Delis (2009) for SWE and Martins et al. (2015) for GWM.

PDWAVE

The PDWAVE is based on the diffusive wave equations without inertia by neglecting all the acceleration and pressure terms.

$$\boldsymbol{U} = \begin{bmatrix} h \\ 0 \\ 0 \end{bmatrix}, \mathcal{F}(\boldsymbol{U}, x, y) = \begin{bmatrix} uh & vh \\ 0 & 0 \\ 0 & 0 \end{bmatrix} \tag{5}$$

The momentum equations use only the source terms presented in Equations (2) and are therefore:

$$\mathcal{S}(\boldsymbol{U}, x, y) = 0 = \begin{bmatrix} -\left(B_x - un^2|\boldsymbol{u}|h^{-4/3}\right) \\ -\left(B_y - vn^2|\boldsymbol{u}|h^{-4/3}\right) \end{bmatrix} \tag{6}$$

where the modulus of the depth-averaged flow velocity vector $|\boldsymbol{u}|$ is given by:

$$|\boldsymbol{u}| = \frac{h^{2/3}\left(\left[\frac{d(h+z)}{dx}\right]^2 + \left[\frac{d(h+z)}{dy}\right]^2\right)^{1/4}}{n} \tag{7}$$

Herein the equations are discretized in an unstaggered structured grid. A finite volume explicit scheme with cell centred control volumes is used. The time step increment is controlled by CFL condition, which is proportional to Δx^2 (Leandro et al., 2014a). PDWAVE uses a prediction correction Wet-Dry front treatment that restricts the movement of water in case of negative depths, obtaining absolute mass conservation (Leandro et al., 2014a).

Sewer Model

SIPSON (Djordjević et al., 2005) is a well established model that solves the full dynamic Saint-Venant equations in the pipes in the form

$$\frac{\partial z}{\partial t} + \frac{1}{B}\frac{\partial Q}{\partial x} = 0 \tag{8}$$

$$\frac{\partial Q}{\partial t} + \frac{\partial(Q^2/A)}{\partial x} + gA\frac{\partial z}{\partial x} + gAS_f = 0 \tag{9}$$

where the values are related to a cross-section located at the coordinate x at time t with z as the water level, B the surface width, Q the discharge, S_f the friction slope and A the area. g is the gravitational constant. The node mass and energy conservation equations are also solved using Equations (10):

$$A_n\frac{\partial z_n}{\partial t} = q_n + \sum_{m=1}^{M} Q_m, \qquad z + \frac{u_{cs}^2}{2g} = z_n \pm K\frac{u_{cs}|u_{cs}|}{2g} \tag{10}$$

where A_n is the horizontal area of the node, z_n the water level in the node, q_n the external inflow/outflow, u_{cs} the cross-sectional average velocity at pipe end and K the local energy loss coefficient, m the pipe index, and M the total number of pipes. The partial differential equations are solved using the Preissmann four-point implicit finite differences scheme. The resulting matrix is solved with the conjugate gradient method. In case of surcharge, SIPSON uses the Preissmann open-slot concept (Preissmann, 1961) where the pressurized flow is simulated using the Saint-Venant equations with a virtual slot placed on top of the pipes. SIPSON model was chosen for the 1D sewer computations due to a lower computational time when compared to explicit 1D models and an unconditional stability.

Linkage Model

The geometric connection between the major and the minor systems is made assuming a direct connection between a surface cell and the sewer manhole through the manhole. The assumption implies that the manhole covers are displaced allowing free flow in both directions. Moreover, although the high resolution DTM provides detailed terrain information, the exact overlapping of the cell centre and the manhole centre is practically impossible. Our approach searches for surface cells nearest to the manhole to link the overland and the sewer models, i.e. the surface cell linked is the one with the minimum distance to the manhole centre. Sometimes this distance is not the best indicator, therefore a second criterion that considers all points within +10% of the distance of the closest point is included to find the one

with the minimum elevation difference to the manhole crest for linking to the sewer model. The algorithm is therefore:

$$Dist_{PQ} = \sqrt{\left(x_{MhoQ} - x_{Surf_P}\right)^2 + \left(y_{MhoQ} - y_{Surf_P}\right)^2} \wedge Link_{Q1} = \min_{P}\left(Dist_{PQ}\right) \forall P \in R$$

(11)

$$z_{PQ} = \sqrt{\left(z_{MhoQ} - z_{Surf_P}\right)^2} \wedge Link_Q = \min_{1.1 Link_{Q1}}\left(z_{PQ}\right) \forall P \in R \tag{12}$$

where R is the set of points in the 2D model, P is a generic point in 2D, Q is a generic manhole, x_{MhoQ} is the x coordinate of the manhole Q, y_{MhoQ} is the y coordinate of the manhole Q, z_{MhoQ} is the z coordinate of the manhole Q, x_{Surf_P} is the x coordinate of the Surface point P, y_{Surf_P} is the y coordinate of the Surface point P, z_{Surf_P} is the z coordinate of the Surface point P, $Dist_{PQ}$ the minimum Euclidean distance, z_{PQ} the difference between elevations, $Link_{Q1}$ is the surface point obtained in the first proximity criterion, and $Link_Q$ is the final linking point.

Although the proximity search is effective, usually there is disagreement between the terrain elevation data obtained from the DTM and the corresponding manhole cover elevation from the sewer network data (Chen et al, 2007). If the crest is lower than the surface the maximum is used as the value for both the surface and the crest. The assumption that the crest elevation is defined differently from the surface elevation is also viable since the cell area might be high and ponding occurs; the ponding can be simulated by elevating the crest or lowering the surface, thus allowing retention.

The interacting discharge rates between the sewer and the overland systems can be defined in a variety of forms, herein it is solved by using orifice, free weir or submerged weir equations, based on the depth and the direction of the flow (Chen et al, 2007). Four exchange scenarios can be defined: (1) Flow from the surface to the manhole with free surface; (2) Flow from the surface to the surcharged manhole; (3) Flow from the manhole to the surface with water level below the crest; (4) Flow from the manhole to the surface with water level above the crest. These conditions are described by the following three equations:

$$Q_{eq} = C_w P_{Mho}\sqrt{2g}\sqrt{\delta z_{Up}^3} \quad if \quad z_{Up} > z_{Crest} > z_{Down} \tag{13}$$

$$Q_{eq} = C_w P_{Mho}\sqrt{2g}\sqrt{\delta z}\delta z_{Up} \quad if \quad \left(z_{Up} \wedge z_{Down}\right) > z_{Crest} \wedge A_{Mho}/P_{Mho} < \delta z_{Up} \tag{14}$$

$$Q_{eq} = C_o A_{Mho}\sqrt{2g}\sqrt{\delta z} \quad if \quad \left(z_{Up} \wedge z_{Down}\right) > z_{Crest} \wedge A_{Mho}/P_{Mho} \geq \delta z_{Up} \tag{15}$$

with

$$z_{Up} = \max\left(z_{Surf}, z_{Mho}\right), \quad z_{Down} = \min\left(z_{Surf}, z_{Mho}\right), \quad \delta z_{Up} = \max\left(z_{Up} - z_{Crest}, 0\right), \quad \delta z = \max\left(z_{Up} - z_{Down}, 0\right) \tag{16}$$

where Q_{eq} is the exchange flow, z_{Mho} is the head inside the manhole, z_{Surf} the surface flow elevation , z_{Crest} the crest elevation, z_{Up} the maximum value between the surface water level

and the manhole head, and z_{Down} the minimum value between the surface flow elevation and the manhole head, C_w is the weir coefficient, C_o the orifice coefficient, A_{Mho} the manhole area, P_{Mho} the manhole perimeter, g the gravitational constant, z_{Mho} the head inside the manhole, z_{Surf} the surface flow elevation, and z_{Crest} the crest elevation. In order to prevent excess drainage and signal inversion on the discharge two discharge limiters are imposed:

$$Q_1 = \frac{\partial z_{Up}}{\partial t} A_{Up}, Q2 = \frac{\partial z}{\partial t} \frac{A_{Up} A_{Down}}{(A_{Up} + A_{Down})} \tag{17}$$

with

$$A_{Up} = \max(A_{Surf}, A_{Mho}), \ A_{Down} = \min(A_{Surf}, A_{Mho}) \tag{18}$$

where A_{Surf} is the area of the surface cell connected to the manhole, and A_{Mho} is the area of the manhole. The discharge between the surface and the sewer system is therefore:

$$Q_{\Delta t_{Link}}^t = \zeta\left(\min(Q_1, Q_2, Q_{eq})\right), with \ \zeta = \frac{z_{Surf} - z_{Mho}}{|z_{Surf} - z_{Mho}|} \tag{19}$$

where, the discharge is assumed positive from the surface to the sewer and negative otherwise.

The surface and sewer flow models have different time steps. The sewer model is implicit and the surface model is explicit. The coupling of models with different time-steps is done for each linked cell by solving the sewer and the surface models sequentially. The values calculated from the sewer model are linearly interpolated and used as the interior boundary conditions for the surface model (Figure 1). The mass conservation is:

$$\frac{\partial z_{Link}}{\partial t_{Link}} = \frac{\partial z_{1D}}{\partial t_{1D}} + \frac{Q_{\Delta t_{Link}}^t}{A_{1D}} \tag{20}$$

And in the surface model:

$$\frac{\partial h_{2D}}{\partial t_{2D}} = \frac{Q_{\Delta t_{Link}}^t}{A_{2D}} \tag{21}$$

This formulation allows the model to interpolate intermediary values that reduces the oscillation which can occur between the two models. Applying a first order finite differences numerical scheme one obtains for updating 1D manhole head:

$$z_{Link}^{t+1} = z_{Link}^t + \frac{z_{1D}^{t+1} - z_{1D}^t}{\Delta t_{1D}} + \frac{Q_{\Delta t_{Link}}^t}{A_{1D}} \Delta t_{2D} \tag{22}$$

and for updating the surface elevation:

$$h_{2D}^{t+1} = z_{2D}^t + \frac{Q_{\Delta t_{Link}}^t}{A_{2D}} \Delta t_{2D} \tag{23}$$

where z_{1D} is the head in the manhole (1D sewer model), h_{2D} the depth in the overlapping 2D mesh call of the surface model, t the previous time step, $t+1$ the time step intended to be updated, z_{Link} the sewer model head estimation after n Δt_{2D} time-steps, $Q_{\Delta t_{Link}}^t$ the discharge calculated through Equation (19) , Δt_{2D} the surface model time step, Δt_{1D} the sewer

model time step, A_{1D} the area of the Manhole, and A_{2D} the area of the cell connected. A maximum time-step for the surface model is enforced as the sewer model time-step. The linkage at correct time steps is assured by limiting the time step in the surface model to the time needed to reach the linkage time. Figure 1 summarises the method used for each Linking time step.
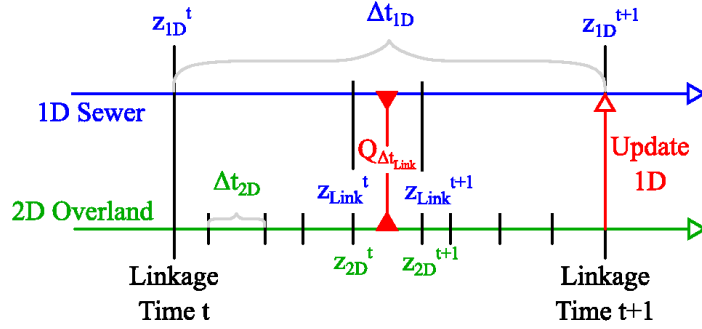

Figure 1 - Synchronization and calculation scheme between the sewer model and overland flow models. z_{1D} is the head in the manhole (1D sewer model), h_{2D} the depth in the overlapping 2D mesh call of the surface model, t the previous time step, $t+1$ the time step intended to be updated, z_{Link} the sewer model head estimation after n Δt_{2D} time-steps, $Q^t_{\Delta t_{Link}}$ the discharge calculated through Equation (19) , Δt_{2D} the surface model time step, Δt_{1D} the sewer model time step, A_{1D} the area of the Manhole, and A_{2D} the area of the cell connected.

We assume the interacting flow between both sewer and surface is vertical such that no horizontal momentum is exchanged. Therefore, the velocity correction for the water surcharging from the sewer and the horizontal surface momentum for the water draining to the sewer are corrected. We get therefore:

$$uh_{2D} = \Gamma_{2D}uh_{2D}, \quad vh_{2D} = \Gamma_{2D}vh_{2D} \tag{24}$$

$$\Gamma_{2D} = \begin{cases} \dfrac{1}{1-\dfrac{Q^t_{\Delta t_{Link}}\Delta t_{2D}}{A_{2D}h_{2D}}} & if & h_{2D} > 0 \\ 0 & if & h_{2D} = 0 \\ 0 & if & Q^t_{\Delta t_{Link}}\Delta t_{2D} \pm \varepsilon_{wd} = A_{2D}h_{2D} \wedge z_{Surf} > z_{Mho} \end{cases} \tag{25}$$

ε_{wd} is the wet and drying threshold constant assumed here as 10^{-6}.

Model comparison indicators

The three modelling approaches and the linkage performance were compared using three different indicators, which rely mainly on the depths, heads and discharges in the linkages and on the surface. The first measure is the total water volume exchanged between surface and sewer system, which allows a global comparison between all three models. The second comparison is based on the hydraulic head and flow rates at linked manholes, allowing detailed observation of the flow interaction between the sewer and the surface systems. The third indicator analyses the inundation extent data to indicate the main differences in overland flow propagation. Average Δt used for GWM was 0.141, for SWE 0.111 and for PDWAVE 0.01.

In PDWAVE Δt was set as 0.01 s. The CFL coefficient and Manning's Roughness coefficient were kept constant as 1 and 0.03, respectively.

Volume exchanged

The first indicator compares the cumulative volume exchanged (i.e. the total volume stored on the surface) and the volume exchanged every 60 s to provide a global view of the system. The relative difference between models is calculated as (Equation 26):

$$\varepsilon_{A,B} = \frac{|2(A-B)|}{A+B} \tag{26}$$

where A represents the first model volume and B the second model volume. As seen, there is no assumption that any of the models is correct so an algebraic average value is considered to be the denominator in the difference formulae.

Hydraulic Head and Discharge Rates

The second indicator is based on the comparison of the head and discharge rates at linked manholes. The necessity to quantify the agreement between the models leads us to use three common statistical coefficients, namely: Percent Bias (PBIAS) (Gupta et al, 1999), Normalized Root Mean Square Error (NRMSE) (Ma et al, 1999) and Pearson product-moment correlation coefficient (C) (Rodgers and Nicewander, 1988). The use of three coefficients is justified due to their imperfections and weaknesses. This allows us to find outliers where only one coefficient would not be able to.

$$PBIAS = \left[\frac{\sum_{i=1}^{n}(z_i^A - z_i^B)}{\sum_{i=1}^{n}(z_i^A)}\right] \tag{27}$$

$$NRMSE = \frac{\sqrt{\frac{\sum_{i=1}^{n}(z_i^A - z_i^B)}{n}}}{(z_{max}^A - z_{min}^A)} \tag{28}$$

$$C = \frac{\sum_{i=1}^{n}(z_i^A - \overline{z^A})(z_i^B - \overline{z^B})}{\sqrt{\sum_{i=1}^{n}(z_i^A - \overline{z^A})^2 \sum_{i=1}^{n}(z_i^B - \overline{z^B})^2}} \tag{29}$$

In equations $PBIAS$, $NRMSE$ and C z_i^A is the $i-th$ result obtained for the variable z, the superscript ^{B} represents values from the model B whilst the superscript ^{A} represents values from the model A the over-line (e.g. $\overline{z^A}$) stands for the average value, the subscript $_{min}$ is the minimum value of the set, the subscript $_{max}$ is the maximum value of the set and n is the total number of elements in the set. $PBIAS$ measures the tendency of the simulated data to be larger or smaller than the experimental or analytical results and range from $-\infty$ to $+\infty$ with 0 as the optimum value. $NRMSE$ measures the average squared difference between simulated and measured data, has values between 0 and 1 with the optimal value of 0. C is the statistical correlation between two sets of data and can have values between 0 and 1 with an optimum value of 1. Since some of the coefficients do not have the permuting property, six combinations were obtained (Namely: SWE vs. GWM, GWM vs. SWE, PDWAVE vs. GWM, GWM vs. PDWAVE, PDWAVE vs. SWE, SWE vs. PDWAVE). Some

nodes were chosen amongst all the nodes for their representation of the full domain and to best illustrate the correlations between the models.

Inundation Extents and Model Predominance

The third indicator is based upon flood depths and extents in the overland flow models.

The global analysis was made computing the difference between the variables for each time step. The standard deviation for the differences for each time step was then computed and the positive 95% confidence interval, assuming that the data had a normal distribution, was computed through Equation (30).

$$\delta_{95\%} = \bar{x} + 1.96\sigma \tag{30}$$

In order to evaluate the spatial predominance of a model in the surface flow, the average depth in time was calculated for each cell i and for each model j $(\overline{\lambda_j(i)})$. The averaged values were then divided by the sum of all models depth for that cell $\sum_{j=1}^{3} \overline{\lambda_j(i)}$, floored to the nearest integer and transformed into a RGB scale where:

$$RGB = \left\lfloor \frac{3\overline{\lambda_1(i)}}{\sum_{j=1}^{3} \overline{\lambda_j(i)}} \right\rfloor \hat{R} + \left\lfloor \frac{3\overline{\lambda_2(i)}}{\sum_{j=1}^{3} \overline{\lambda_j(i)}} \right\rfloor \hat{G} + \left\lfloor \frac{3\overline{\lambda_3(i)}}{\sum_{j=1}^{3} \overline{\lambda_j(i)}} \right\rfloor \hat{B} \tag{31}$$

$$\sum_{j=1}^{3} \overline{\lambda_j(i)} = \overline{\lambda_1(i)} + \overline{\lambda_2(i)} + \overline{\lambda_3(i)} \tag{32}$$

$$\lambda_1(i) = h_{PDWAVE}(i), \lambda_2(i) = h_{GWM}(i), \lambda_3(i) = h_{SWE}(i), \forall i \in Cells \tag{33}$$
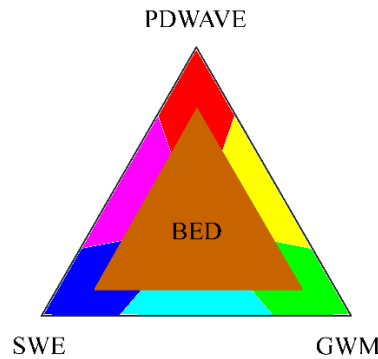

Figure 2 - RGB model predominance

This novel methodology of the comparison between three models through RGB scale results in an image that shows, as a combination of 6 colours, the predominance of the model in a region (Figure 2). A red region in Figure 2, for example, shows that the modelled average depth in PDWAVE is higher in that region than the average value of the three models. A cyan shows that GWM and SWE are in average higher that the average of the three models. This method allows a division of the domain in several areas with similar behaviours to better characterise the flow based on the predominant model or models. With this data it was possible to plot a $x - y$ scatter plot in which each cell is represented by its depth in two models at a time (x axis for one model and y axis for another). These points are then coloured with the area colours, based on the area they belong to, allowing an insight on the difference for each cell in each area.

The maximum depths were also plotted along with the differences between them to point out to the major differences and damp the minor ones.

Lastly, a coefficient that assumes no correct model is applied. A Ξ_m coefficient is introduced and suggested for comparing the extents of all modelling results:

$$\Xi_m = \frac{\varphi_{w,w} - (\xi_{w,d} + \xi_{d,w})}{\varphi_{w,w} + \xi_{w,d} + \xi_{d,w}}$$ (33)

where, $\varphi_{w,w}$ is the number of common wet cells, $\xi_{w,d}$ the number of wet cells in the 1st model that are dry in other models, and $\xi_{d,w}$ the number of dry cells in the 1st model that are wet in the other models. This coefficient provides a penalty for the erroneous cells (cells that have different values in each model) by subtracting them in the numerator. The Ξ_m coefficient varies from -1 to 1, where 1 is a perfect fit, 0 when the number of correctly and erroneously predicted cells is equal, and -1 for the case that all cells differ. In the study, we aim to compare the difference between all the models without assuming either as correct, hence the use of Ξ_m. The depth value of 0.001 m was considered the threshold as the value to consider a cell as wet or dry.

Case study

The case study area used herein is located in Keighley, Bradford, in the UK. The catchment area is characterized by slopes that vary from 0.14% to 2.44% with an average of 1.33% (Leandro et al, 2009) and elevations from 82 to 105.12 m (Figure 3). The storm water drainage system in this area consists of 90 pipes and 90 manholes and 1 outlet. The 2D model is based on 2 × 2m grid cells obtained from a DEM of the location. Boundary conditions were defined as vertical walls to eliminate boundaries as a source of instabilities. A total of 84 links connect the surface with the storm water drainage system with capability of bidirectional flow (Dual Drainage). The simulation was based on a synthetic block rainfall of 42 mm in one hour, introduced directly in SIPSON's manholes as a hydrograph calculated based on the catchment area through the runoff module BEMUS (Maksimovic et al, 1995), which corresponds to a 100-year return period event for that region. The simulation was run for 6 h.
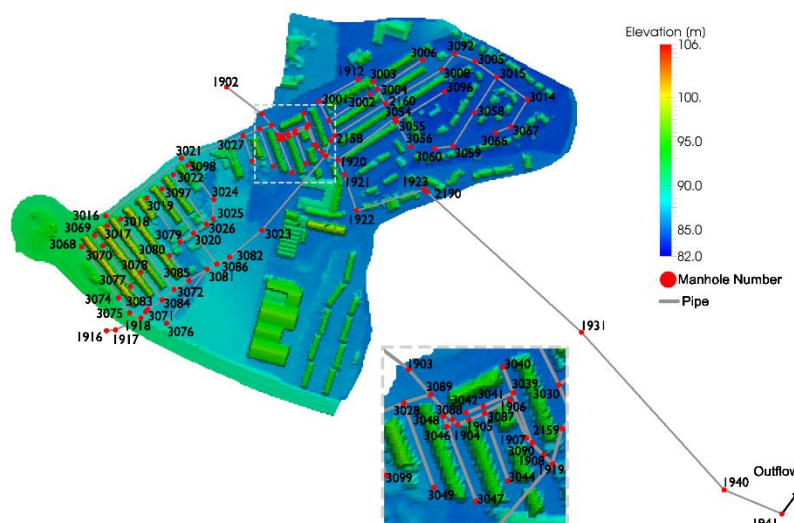

Figure 3 – Case study topology and bed elevation

Results and Discussion

The comparison of the three overland flow models under dual drainage framework will be made using three different set of parameters. The computational time was approximately 188 min, 183 min, and 284 min for PDWAVE, GWM and SWE respectively.

Volume exchange between sewer and overland flow models

Both the surface and the storm water drainage systems influence the volume exchanged. The results obtained for PDWAVE, GWM and SWE are presented in Figure 4: namely the cumulative volume exchanged (left) and the volume exchanged overtime in intervals of 60 s (right).
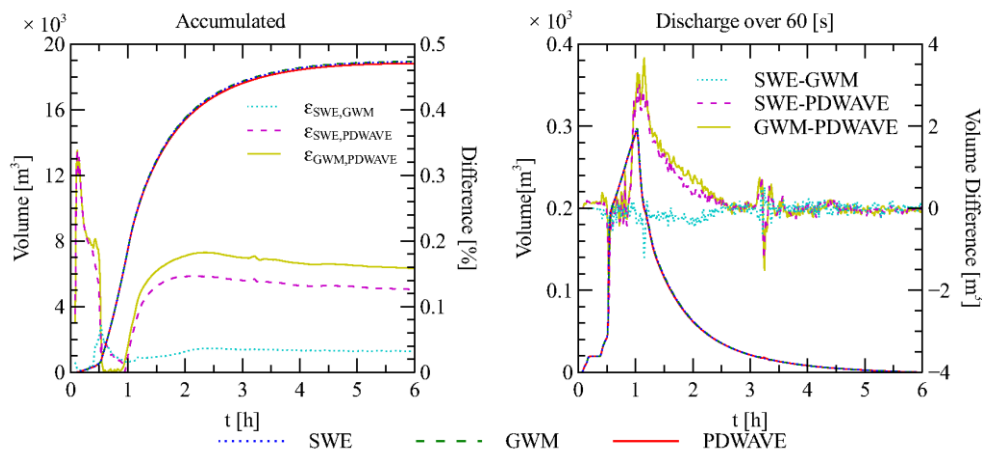
Figure 4 - Exchanged water volume between the sewer and surface systems (left) Cumulative, (right) discharged volume over Δt = 60 s

The left vertical axis represents the value for each overland flow model whilst the right vertical axis indicates the differences between the models. The results in Figure 4 show close agreement. To be noticed that the difference between models is presented in absolute value. Since GWM has the higher volume on the surface, the difference between GWM and PDWAVE is higher than between PDWAVE and SWE. The peaks obtained in the first half hour are mainly due to PDWAVE's smaller wave speed propagation when compared to GWM and SWE. As such there is a higher depth on top of the manhole and therefore a smaller exchange. The values of the accumulated volume on the left image are almost superimposed and the differences are small. The difference ($\varepsilon_{A,B}$) at the end of the simulation is below 0.16% for all surface models, which is a good agreement. The difference between SWE and GWM is smaller than the one between PDWAVE and the other two models.

Right image shows the discharged volume every 60 s. The differences are very small and the volume is almost coincident. In detail, the difference between the models is shown in the right vertical axis. The major difference, found at t ≈ 1 h, are relatively small: 4 m^3 difference for a discharged volume of 300 m^3. Figure 4 also shows that the cumulative discharge is higher in SWE and GWM than in PDWAVE. When the discharge is above 500 m^3 GWM tends to have a slightly bigger discharge, as seen by the negative values of volume difference.

Hydraulic Head and Discharge Rates at the Linked Manholes

The statistical coefficients presented in section Hydraulic Head and Discharge Rates for hydraulic head and discharge rates for the manholes are plotted in Figure 5. The figure is divided into six figures. $PBIAS$(27), $NRMSE$(28) and C(29) are plotted in the three columns sequentially. The top row represents the manhole head and the bottom row for the discharge. Each figure holds the six combinations mentioned earlier. The model results were subtracted (i.e for example, A in Equations (27), (28) and (29) is substituted by SWE, and B by PDWAVE) for all the manholes and all the combinations. The resulting values are plotted comparing the results for each model (for example, A=SWE, B=GWM in the x axis and A=SWE, B=PDWAVE in the y axis).
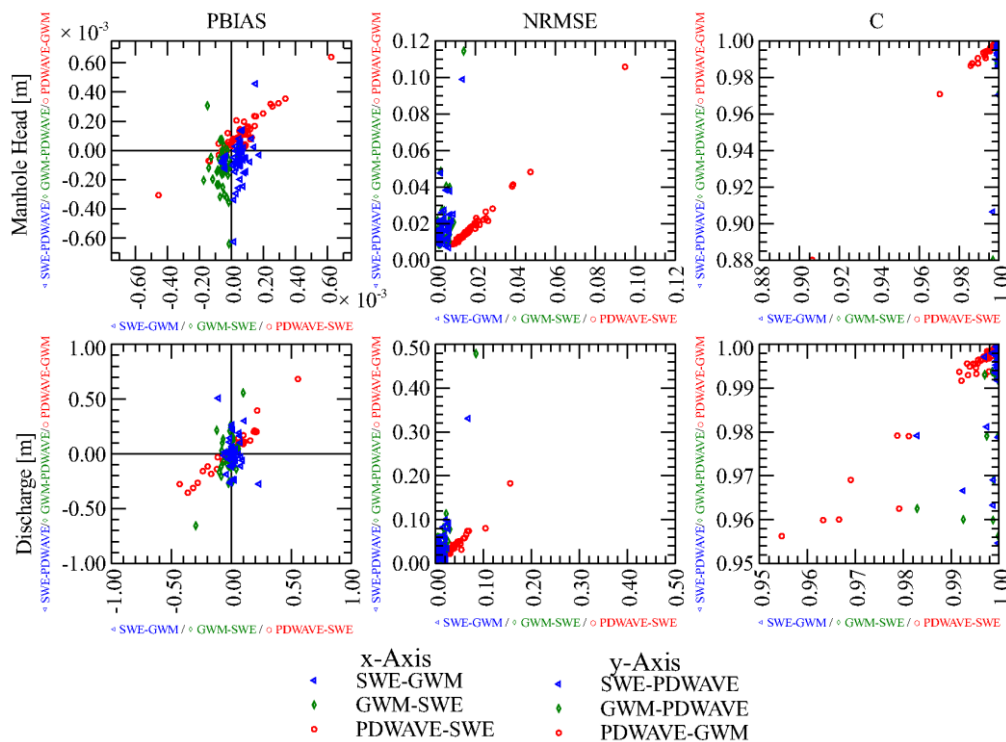
Figure 5 - Comparison of the manhole head and discharges between all the overland flow models using $PBIAS$(27), $NRMSE$(28) and C(29) Coefficients

In Figure 5, PDWAVE has higher hydraulic head for most of the manholes among all models. This trend can be seen in PBIAS Manhole Head since most of the coefficients for PDWAVE are positive on x and y axis. This is reinforced by the negative values for GWM and SWE when compared to PDWAVE (y axis). As a consequence of higher head and due to the surcharging flow, PDWAVE also has higher discharges for the majority of the manholes when compared to GWM and SWE. It should be noticed that the differences are kept well within reasonable limits (<5%) for the vast majority of the manholes.

$NRMSE$ provides an insight on the relative global difference for the manhole head as a percentage. Most of the manhole heads have a very good agreement and are kept well below 0.03 (3% difference) with GWM and SWE relation below 0.01. Points with notable differences are always below 0.12. The discrepancies in discharge the discrepancies are larger. Values are

usualy kept below 0.08. There is a tendency of PDWAVE to distance itself from both GWM and SWE as seen by an almost $x = y$ line formed by the markers present in the discharge and head, and except for some outliers the relation between GWM and SWE is usualy less than 0.02.

C values are with a very good agreement. Manhole heads are kept within a correlation higher than 0.975 with the exception of only a few points. The same holds for the discharges, showing a very good correlation between all the datasets. It should be noticed that the GWM vs. SWE and SWE vs. GWM relations have considerably higher correlations than the ones with PDWAVE involved with the lower value of 0.995 for the head and 0.98 for the discharge.

Some nodes were chosen amongst all nodes for their representation of the full domain and to best illustrate the correlations between the models and are presented in Table 1 and Figure 6. Figure 6 top row shows the head for each represented manhole whereas the bottom row presents the discharge. A positive discharge represents a surface to sewer discharge whilst a negative one shows a surcharge from the sewer system.

Table 1 - Manhole elevation, 2D models elevations, and $NRMSE$ correlation coefficients for the selected nodes (2190, 3056, 3004, 3079, 1912, and 3067)

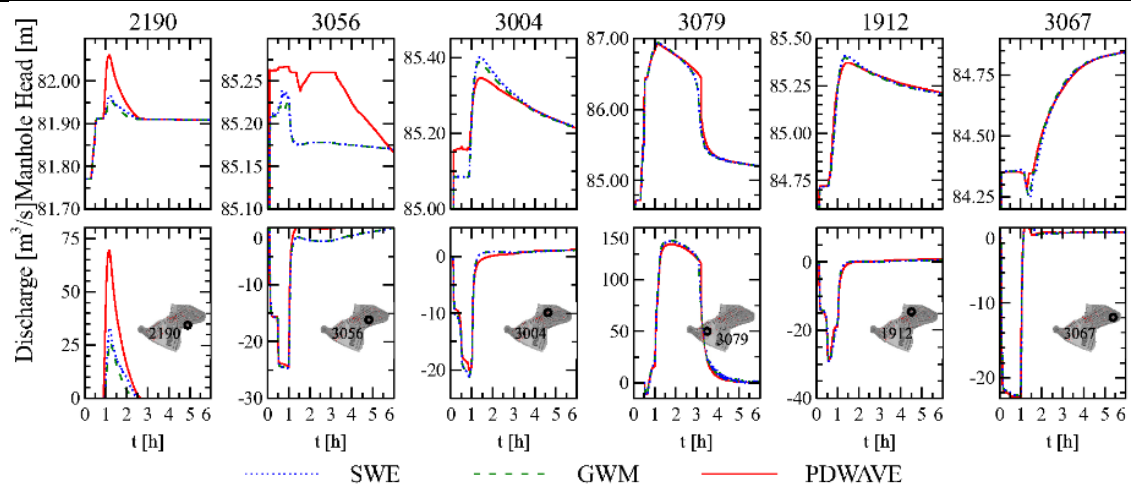|				2190	3056	3004	3079	1912	3067
	Elevation	[m]	PDWAVE	85.33	85.26	85.15	86.42	84.55	84.27
			GWM and SWE	85.37	85.16	85.07	86.42	84.68	84.35
			Manhole Bottom	81.688	84.25	83.69	84.72	83.6	83.507
			Manhole Crest	85.368	85.132	85.085	86.38	84.718	84.347
NRMSE	Head	[-]	SWE vs. GWM	0.0139	0.0026	0.0029	0.0053	0.0036	0.0064
			SWE vs. PDWAVE	0.1067	0.0481	0.0193	0.0394	0.0152	0.0194
			GWM vs. PDWAVE	0.1003	0.0479	0.02	0.0401	0.0157	0.0197
			Average	0.0736	0.0329	0.0141	0.0283	0.0115	0.0152
	Balance	[-]	SWE vs. GWM	0.0764	0.0018	0.0025	0.0129	0.0033	0.0028
			SWE vs. PDWAVE	0.4048	0.0571	0.0299	0.0313	0.0203	0.0084
			GWM vs. PDWAVE	0.1693	0.0578	0.0316	0.0328	0.0202	0.0083
			Average	0.2168	0.0389	0.0213	0.0257	0.0146	0.0065

Figure 6 - Manhole Head and Discharges for the selected nodes (2190, 3056, 3004, 3079, 1912, and 3067)

Node 2190 has some of the major differences between models with regard to discharges. The maximum difference between PDWAVE and the other models is 0.1 m and the discharge 0.04 m^3/s. The manhole head is solely changed by the sewer system and discharges are from the surface to the manhole as seen in the right figure. The major differences are explained by a 0.04 m difference (see Table 1) on the surface between PDWAVE and the other models. Between GWM and SWE the difference is considerably smaller and is in full scale due to the surface flow. The maximum difference in discharge is small and lower than 0.005 m^3/s, which is a good agreement.

Node 3056 shows the worst correlation regarding manhole heads. The difference is relatively small, 0.05 m and can be easily explained by a difference in the surface elevation as shown in Table 1. The difference is of 0.1 m. The discharge is controlled by not only the manhole head but also the differences between the elevation on the surface and the manhole head. This shows that the surface flow elevation is smaller in GWM and SWE.

Node 3004 has 0.08 m difference in the surface elevation between PDWAVE and the other models, besides this difference, the surface crest is in between these values. These differences force a higher water level in PDWAVE as seen in the beginning of the manhole head figure and a lower level in GWM and SWE. The head of the manhole is therefore very close to the manhole crest elevation in GWM and SWE and to the surface elevation in PDWAVE. PDWAVE has some oscillations as a small part of the flow is retained in the surface and directly influences the manhole head. GWM and SWE have a small difference in elevations between the crest and the surface that allows the flow to leave the cell without disturbing the manhole therefore the head inside the manhole is always the crest elevation and all the flow that would increase the manhole head is expelled to the surface. This situation increases the discharge as seen in the right figure during the first hour. After the first hour, the discharge diminishes and the head increases as a direct influence of the surface flow inverting the flow from a surcharge to a discharge.

Node 3079 is one of the few nodes where the flow is truly bidirectional. The manhole crest is at 86.38 m whilst the surface is at 86.42 m for all models. The discharge only happens when the manhole hydraulic head exceeds the surface water level and the behaviour of all models is similar. The results almost overlap except for the descending branch where GWM and SWE have a smoother transition. This transition is due to the influence of the sewer network as there is a faster decrease of head for GWM and SWE. Eventually the models return to similar values since all the flow that arrives at the cell is drained to the sewer. Some discharge oscillations are seen in GWM and SWE after 3 h. The unsteady nature of both models can explain this as some oscillations occur in the surface flow. The discharge in GWM and SWE is also slightly higher than in PDWAVE.

Node 1912 is controlled by the manhole head and is therefore a good indicator of the global changes until 30 min. Afterwards the differences reflect the flow over the manhole. PDWAVE achieves a faster peak whilst GWM and SWE achieve a higher head peak. The discharges are almost overlapping with some small differences that are a reflection of the head in the manhole.

Node 3067 also shows consistency between data as shown in Table 1 for $NRMSE$ of Average Balance and Head. The elevations are very similar, with only a small divergence for 3067 when the head becomes lower than the crest resulting from a global sewer system response. The oscillations seen are due to the proximity of the crest to the surface elevation in the SWE and GWM whilst for PDWAVE the manhole crest is 0.08 m higher than the surface.

Overall the results are in very good agreement with some major differences explained by the different discretization and some small differences attributed to the models. The manholes head and discharges are very similar between models. The results also show that an equal representation of the surface and the linkage is of the utmost importance since some major differences can occur due to different representations. As expected GWM has closer results to SWE than PDWAVE. This is due to the differences in the governing equations but also on the discretization. Indeed GWM and SWE share the same irregular mesh, and therefore the models share the same exact elevations at the surface (Table 1).

PDWAVE on the contrary uses a regular grid, and therefore the surface node elevations inevitably differ from the other two models.

Inundation Extents and Model Predominance

The results based on the methodology presented in section Inundation Extents and Model Predominance are shown in Figure 7. In the left the RGB predominance analysis and the right the area subdivision obtained from the analysis.
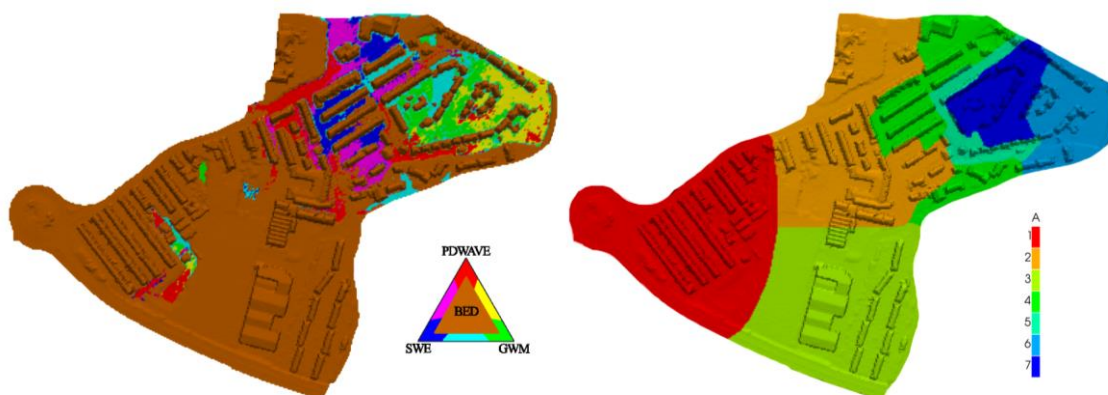

Figure 7 - Left: spatial model predominance; Right: Subdivision of the domain based on the spatial model predominance analysis

Figure 7 shows that there is no dominant model as the distribution has roughly the same area for all the models. PDWAVE has predominance upstream. This is also seen near the manhole with the highest discharges showing that PDWAVE tends to "retain" more water upstream opposed to GWM that shows higher depths downstream due to a higher but slower wave front.

Major differences were found in the period from 50 min to 110 min with a maximum at 80 min of ≈0.11m (Figure 8). The results were plotted for 50, 80, 110 min and the maximum depth in each cell and are presented in Figure 8.

Figure 8 shows the direct comparison between all the models tested for the three time steps mentioned along with the maximum extent. The figure is arranged so that the time steps are presented in columns and the comparison in rows. In each figure, the horizontal axis represents model 1 and the vertical axis for model 2. This is assessed by the first and second model in the rows header. Two functions based on Equation (30) where plotted. This two functions imply that between them there is a 95% confidence that any value of model 1 is within $2\delta_{95\%}$ of model 2. Each dot represents a cell depth for the compared models and the colour the area where the point is.
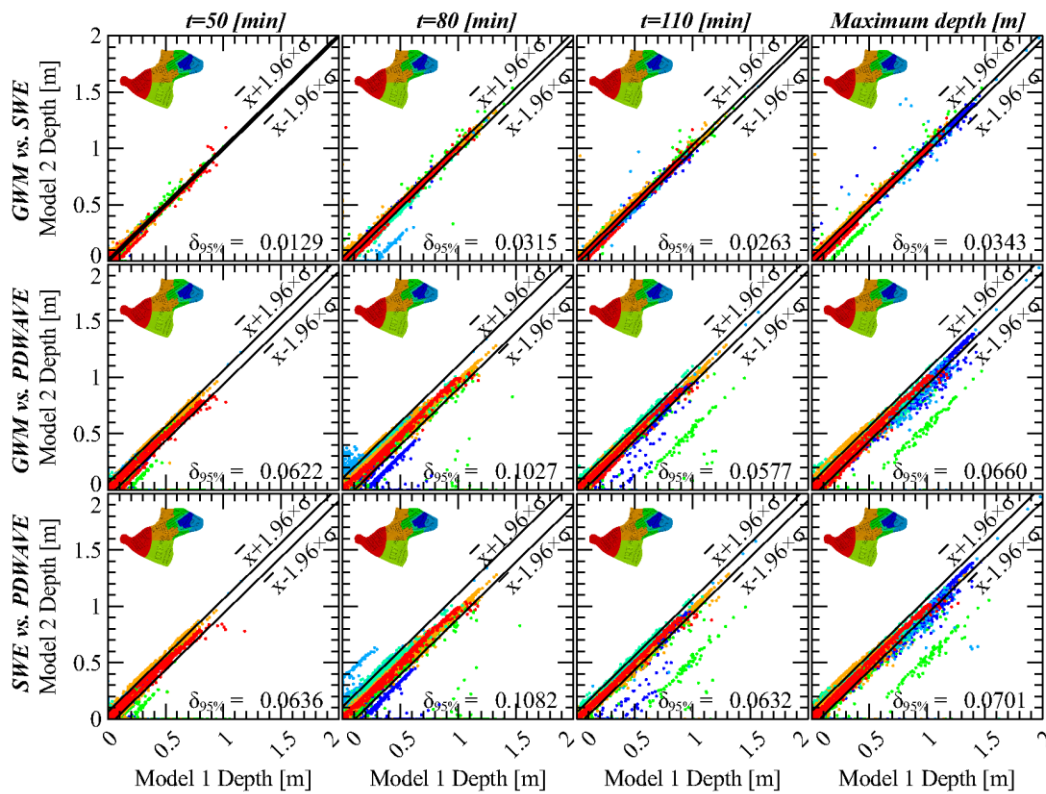
Figure 8 - Comparison of the cell flood-depths flooded in both models for t=(50, 80, 110) min and maximum depth. , where $\delta_{95\%}$ is the 95% confidence interval between analysed models in m. Upper and lower limits shown in black lines.

The analysis from Figure 8 shows a high correlation for GWM vs. SWE. For 50th minute the red area shows a small difference in depth as GWM has a higher depth than SWE. The vast majority of points is near the origin and the values are very similar between themselves. The points then spread through $x = y$ line showing a very good relation. The 80th minute is when the differences between the models is larger. The confidence interval is larger with $\delta_{95\%}$ except for the maximum extent and some areas show slight disagreement, namely the area shown in cyan. This area has a flow with up to 30 cm difference and the difference is due to no loss in the momentum when the flow goes over a small bump in the south-east of the area. The red and light green area also shows some differences, in the magnitude of 10 cm once again due to a slower but higher depth of propagation by GWM. Minute 110, with the exception of some scattered points shows a slightly higher spread than minute 50 but with a larger concentration of wet cells. Red, cyan, blue and orange stand out as the areas with the

most differences. This difference is however of small magnitude with higher values of about 10 cm.

GWM vs. PDWAVE (Figure 8) has a larger difference than GWM vs. SWE. At 50 min the results, although more scattered than SWE vs. GWM show a good agreement and the spread is kept within 15 cm. The most noticeable areas are the red and dark green. The red area is kept within reasonable limits except for some points that lay outside the confidence interval, for the dark green area, some points with water show difference up to 20 cm. GWM predicts some flooded areas that PDWAVE does not that can have differences up to 80 cm in the green and orange area. For the 80th minute the differences increase. Light blue areas are now predicted higher in PDWAVE than GWM and Blue, and green areas higher in GWM than PDWAVE. This is a direct outcome of the mesh discretization. Flow is restricted in some areas due to the structured mesh of PDAWAVE thus routing the flow through the cyan area to the light blue whilst for GWM the flow runs through cyan to dark green. Red area is stable and with a very high resemblance. At 110 min the scatter is diminished and the depth start to converge as flow arrives. GWM flooded point that had no depth in PDWAVE start now to get flooded in dark green area and the points reflect that as they tend to decrease the difference somewhat linearly.

SWE vs. PDWAVE has a similar trend as GWM vs. PDWAVE. The 50 min and 110 min are very similar with the same zones flooded. The main differences reside in the red area, that is more similar between SWE and PDWAVE than GWM and PDWAVE due to less nodes outside the confidence interval. For minute 80 light blue area shows a different tendency than GWM vs. PDWAVE. With still some differences the light blue area shows an increase linearly whilst in GWM vs. PDWAVE there was a complete scatter. This could point to a place where the PDWAVE flow is more similar to SWE than GWM is to SWE.
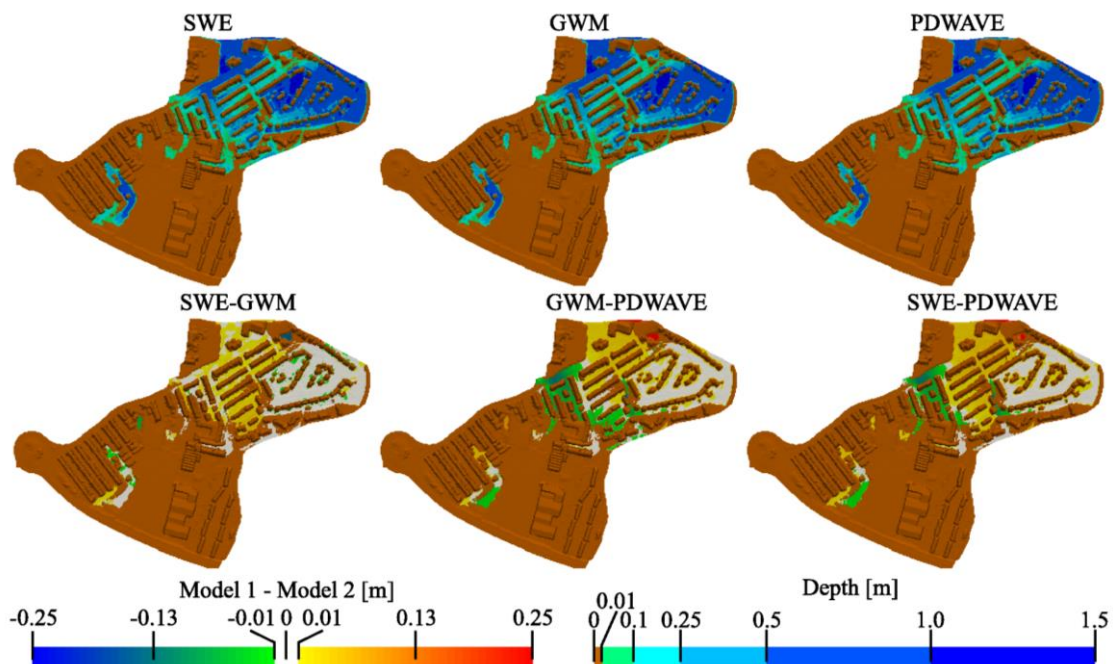

Figure 9 - Comparison of the inundation maps for the maximum depth achieved in the three models and the differences between each models.

The maximum depth and extent have a completely different behaviour of the time series. Instead of capturing the instant it shows the maximum depths for the whole duration (Figure 9). As seen in the maximum extent, all three models present a very similar extent and depths, with some differences. Areas in blue and red have differences of 10 cm and more, whilst yellow and green areas show differences between 10 and 1 cm. White areas have less than 1 cm difference. The differences between SWE and GWM are small as seen by the yellow, green and white colouring on most of the map. Differences are only relevant in the north, where a blue area stands out. The area shows a higher level of GWM of ≈10 cm. The differences between both GWM and SWE, when compared to PDWAVE are very similar. PDWAVE shows higher depths upstream, and a lower difference in red in the north part of the map. The first can be attributed to a slower propagation from PDWAVE that retains some water upstream, however of a very small magnitude as the differences are lower than 20 cm. The latter might be related to the discretization (structured vs unstructured) or bed elevation treatment. The flow might divert to that area when using n unstructured grid whilst for a structured grid the flow is barred. Overall the results for the three models are in a very good agreement.

The total amount of wet and dry cells was computed in time and is shown in Figure 10 left with the vertical axis in log scale. An excellent result happens if the number of coinciding cells is large. In grey one can see that for later times the amount of cells in total agreement (Wet in SWE, GWM, and PDWAVE) is large (more than 10,000). The number of agreeing cells between GWM and SWE is also of a high magnitude as the values are always greater than 100. PDWAVE has however a slight disagreement since the number of wet cells that are not wet in any other model is also high. The number of wet cells that are only wet in one model (SWE and GWM), with the exception already mentioned, is low, along with the number of cells in agreement between SWE and PDWAVE ,and GWM and PDWAVE. This shows a slight disagreement of PDWAVE, however as mentioned earlier it is of relative magnitude.
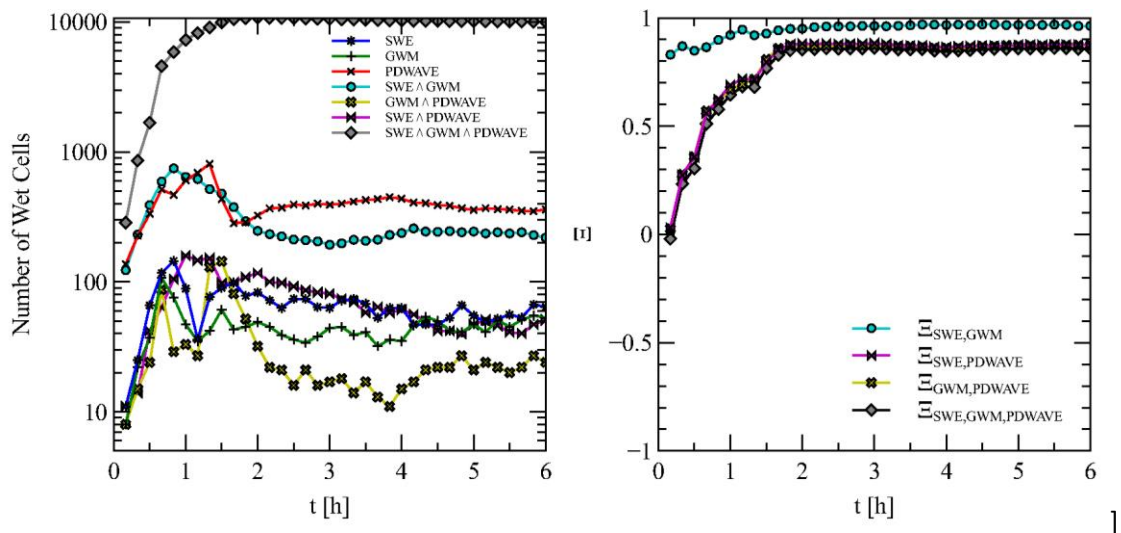

Figure 10 - Left: Number of wet cells in time for each model and each combination of models. Right: Ξ_m Coefficient comparing all combinations of models.

The results on Figure 10 show that for the coefficient in Equation (34) for SWE and GWM is always very high. The comparisons with PDWAVE for both the GWM and SWE show lower coefficient with the number of agreed cells are always larger than the disagreed ones. After 30 min the coefficient surpasses 0.33 which shows that at least twice of the disagreeing cells are in agreement. This is in line with the previous results as all of the models are very similar in extent shown in Figure 9.

Conclusions

In this paper three overland flow models (SWE, GWM and PDWAVE) with different levels of complexity in dual drainage modelling were evaluated and compared using the Keighley test case. To enable a fair overland flow comparison, all three models were coupled with the same fully dynamic sewer network model (SIPSON). A coefficient was used to evaluate the models without assuming either as correct. The linkage is obtained by solving sequentially the sewer and the overland flow models with interpolated discharge values from the sewer model used as internal boundary condition of the surface model. This was based on an exchange formulation that allows for the connection between two models with different time steps by interpolating the discharges and heads.

Three indicators were adopted to compare and verify the agreement between models, namely: (a) a volume exchange between sewer and overland flow models; (b) the hydraulic head and discharge rates at the linked manholes; and (c) the inundation extents and model predominance. A novel methodology based on RGB-scale was used to interpret the results, which was particularly useful for the situation where none of the three set of model results is considered as a benchmark ("accurate") solution.

For this case study (and given the predominance of relatively low slopes), the results are consistent between all coupled models in terms of the extents of flooding, depth and volume exchanged. Nonetheless, it was also shown for the test conducted that the PDWAVE has higher maximum flood depth and has a slower propagation of the flood front. The GWM showed higher depths downstream as the wave front is slower and therefore higher than SWE. Overall the results show a better agreement between GWM and SWE than between PDWAVE and the other models, and the simplified overland models can produce comparable results to fully dynamic models with less computational cost.

Acknowledgements

Please cite: *R Martins, J Leandro, A S Chen, S Djordjević , 2017, A comparison of three dual drainage models: Shallow Water vs Local Inertial vs Diffusive Wave, Journal of Hydroinformatics*

References

Abdullah A.F., Vojinovic Z., Price R.K., Aziz N.A.A. (2012) Improved methodology for processing raw LiDAR data to support urban flood modelling – accounting for elevated roads and bridges. Journal of Hydroinformatics 14(2):253–269 28

de Almeida G.a.M., Bates P. (2013) Applicability of the local inertial approximation of the shallow water equations to flood modeling. Water Resources Research 49(8):4833–4844, DOI 10.1002/wrcr.20366

de Almeida G.a.M., Bates P., Freer J.E., Souvignet M. (2012) Improving the stability of a simple formulation of the shallow water equations for 2-D flood modeling. Water Resources Research 48(5):n/a–n/a, DOI 10.1029/2011WR011570

Aronica G.,Tucciarelli T.,Nasello C. (1998) 2D multilevel model forfloodwave propagation inflood-affected areas. Journal of Water Resources Planning and Management 124(4):210–217

Borsche R., Klar A. (2014) Flooding in urban drainage systems: coupling hyperbolic conservation laws for sewer systems and surface flow. International Journal for Numerical Methods in Fluids 76(September):789–810, DOI 10.1002/fld.3957

Castro M., Ferreiro Ferreiro A., Garcıa-Rodrıguez J., González-Vida J., Macıas J., Parés C., Vázquez-Cendón M. (2005) The numerical treatment of wet/dry fronts in shallow flows: application to one-layer and two-layer systems. Mathematical and Computer Modelling 42:419–439, DOI 10.1016/j.mcm.2004.01.016

Cea, L., Garrido, M., and Puertas, J. (2010). "Experimental validation of two-dimensional depth-averaged models for forecasting rainfall-runoff from precipitation data in urban areas." J. Hydrol., 382(1-4), 88-102.

Chen A., Djordjevic S., Leandro J., Savić D. (2007) The urban inundation model with bidirectional flow interaction between 2D overland surface and 1D sewer networks. In: NOVATECH 2007, pp 465–472

Chen A., Leandro J., Djordjević S., Schumann A. (2015) Modelling sewer discharge via displacement of manhole covers during flood events using 1D/2D SIPSON/P-DWave dual drainage simulations. Urban Water Journal DOI 10.1080/1573062X.2015.1041991

Chertock, A., Cui, S., Kurganov, A., and Wu, T. (2015). Well-balanced positivity preserving central-upwind scheme for the shallow water system with friction terms. International Journal for Numerical Methods in Fluids, 78(6):355–383, doi:10.1002/fld.4023.

Djordjević S., Prodanović D., Maksimović C. (1999) An approach to simulation of dual drainage. Water Science and Technology 39(9):95–103

Djordjević S., Prodanović D., Maksimović C., Ivetić M., Savić D. (2005) SIPSON-simulation of interaction between pipe flow and surface overland flow in networks. Water science and technology 52(5):275–83

Ellis J., McBean E., Mulamoottil G. (1982) Design of dual drainage systems using SWMM. Journal of the Hydraulics Division 108(HY10):1222–1227

Fraga I., Cea L., Puertas J. (2015) Validation of a 1D-2D dual drainage model under unsteady part-full and surcharged sewer conditions. Urban Water Journal, DOI 10.1080/1573062X.2015.1057180

Fernández-Pato, J. and García-Navarro, P. (2016). "2D Zero-Inertia Model for Solution of Overland Flow Problems in Flexible Meshes." J. Hydrol. Eng., 10.1061/(ASCE)HE.1943-5584.0001428, pp 04016038.

Gupta H., Sorooshian S., Yapo P. (1999) Status of automatic calibration for hydrologic models: Comparison with multilevel expert calibration. Journal of Hydrologic Engineering 4(2):135–143, DOI:10.1061/(ASCE)1084-0699(1999)4:2(135)

Hsu M., Chen S., Chang T. (2002) Dynamic inundation simulation of storm water interaction between sewer system and overland flows. Journal of the Chinese Institute of Engineers 25(2):171–177

Lal, A.W. (1998) "Weighted implicit finite-volume model for overland flow." J. Hydraul. Eng., 10.1061/(ASCE)0733-9429(1998)124:9(941), 941-950.

Leandro J., Chen A., Djordjević S., Savić D. (2009) Comparison of 1D/1D and 1D/2D coupled (sewer/surface) hydraulic models for urban flood simulation. Journal of Hydraulic Engineering 135(6):495–504, DOI 10.1061/(ASCE)HY.1943-7900.0000037

Leandro J., Djordjević S., Chen A., Savić D., Stanić M. (2011) Calibration of a 1D/1D urban flood model using 1D/2D model results in the absence of field data. Water Science & Technology 64(5):1016, DOI 10.2166/wst.2011.467

Leandro J., Chen A., Schumann A.(2014a) A2D parallel diffusive wave model for floodplain inundation with variable time step (P-DWave). Journal of Hydrology 517:250–259, DOI 10.1016/j.jhydrol.2014.05.020

Leandro J., Lopes P., Carvalho R., Páscoa P., Martins R., Romagnoli M. (2014b) Numerical and experimental characterization of the 2D vertical average-velocity plane at the center-profile and qualitative air entrainment inside a gully for drainage and reverse flow. Computers & Fluids 102:52–61, DOI 10.1016/j.compfluid.2014.05.032

Leandro J., Schumann A., Pfister A. (2016) A step towards considering the spatial heterogeneity of urban key features inurban hydrology floodmodelling. Journal ofHydrology 535:356–365, DOI10.1016/j.jhydrol.2016.01.060

Liang Q., Marche F. (2009) Numerical resolution of well-balanced shallow water equations with complex source terms. Advances in Water Resources 32(6):873–884, DOI 10.1016/j.advwatres.2009.02.010

Lopes P., Leandro J., Carvalho R., Páscoa P., Martins R. (2013) Numerical and experimental investigation of a gully under surcharge conditions. Urban Water Journal 00(0):1–9, DOI10.1080/1573062X.2013.831916

López-Barrera, D., García-Navarro, P., Brufau, P., and Burguete, J. (2012). "Diffusive-wave based hydrologic-hydraulic model with sediment transport. I: Model development." J. Hydrol. Eng., 10.1061/(ASCE)HE.1943-5584.0000552, 1093-1104.

Ma Q., Smith A., Hook J., Bridges D. (1999) Surface transport of 2, 4D from small turf plots: Observations compared with GLEAMS and PRZM.2 model simulations. Pesticide science 433(June 1998):423–433,DOI 10.1002/(SICI)1096-9063(199904)55:4h423::AID-PS935i3.0.CO;2-B

Mahdizadeh H., Stansby P.K., Rogers B.D. (2011) On the approximation of local efflux/influx bed discharge in the shallow water equations based on a wave propagation algorithm. International Journal for Numerical Methods in Fluids 66(10):1295–1314, DOI 10.1002/fld.2314

Mahdizadeh H., Stansby P.K., Rogers B.D. (2012) Flood Wave Modeling Based on a Two-Dimensional Modified Wave Propagation Algorithm Coupled to a Full-Pipe Network Solver. Journal of Hydraulic Engineering 138(3):247–259, DOI 10.1061/(ASCE)HY.1943-7900.0000515

Maksimović C., Rajcević A., Djordjević S., Prodanović D., Draksović M. (1995) Results of simulation with updated data andmodified Bemus model. In:Calomino F,Maksimović v,Molino B(eds) Urban Drainage Experimental Catchment in Italy, pp 263–276

Martins R., Leandro J., Carvalho R. (2014) Characterization of the hydraulic performance of a gully under drainage conditions. Water science and technology 69(12):2423–30, DOI 10.2166/wst.2014.168

Martins R., Leandro J., Djordjević S. (2015) A well balanced Roe Scheme for the local inertial equations with an unstructured mesh. Advances in Water Resources DOI 10.1016/j.advwatres.2015.07.007

Martins R., Leandro J., Djordjević S. (2016a) Analytical and numerical solutions of the Local Inertial Equations. International Journal of Non-Linear Mechanics 81:222–229, DOI 10.1016/j.ijnonlinmec.2016.01.015,

Martins R., Leandro J., Djordjević S. (2016b) Analytical Solution of the Classical Dam-Break Problem for the Gravity WaveModel Equations. Journal of Hydraulic Engineering 0(0), DOI 10.1061/(ASCE)HY.1943-7900.0001121

Martins R., Leandro J., Djordjević S. (2016c) Influence of sewer network models on urban flood damageassessment based on coupled 1D/2D models. Journal of Flood Risk Management doi:10.1111/jfr3.12244

Nasello C., Tucciarelli T. (2005) Dual multilevel urban drainage model. Journal of Hydraulic Engineering 131(9):748–754, DOI 10.1061/(Asce)0733-9429(2005)131:9(748)

Ponce V. (1990) Generalized diffusion wave equation with inertial effects. Water Resources Research 26(5):1099–1101, DOI 10.1029/WR026i005p01099

Preissmann A. (1961) Propagation des intumescences dans les canaux et rivières. In: Congress of the French Association for Computation

Prodanović D., Djordjević S., Maksimović C. (1998) GIS assisted model for dual drainage simulation. In: Hydroinformatics' 98

Rodgers J., Nicewander W. (1988) Thirteen ways to look at the correlation coefficient. The American Statistician 42(1):59–66, DOI 10.1080/00031305.1988.10475524

Russo B., Sunyer D., Velasco M., Djordjević S. (2015) Analysis of extreme flooding events through a calibrated 1D/2D coupled model: the case of Barcelona (Spain). . Journal of Hydroinformatics 17(3):473–491

Seyoum S., Vojinovic Z., Price R., Weesakul S. (2012) Coupled 1D and Noninertia 2D Flood Inundation Model for Simulation of Urban Flooding. Journal of Hydraulic Engineering 138(1):23–34, DOI 10.1061/(ASCE)HY.1943-7900

Song L., Zhou J., Guo J., Zou Q., Liu Y. (2011) A robust well-balanced finite volume model for shallow water flows with wetting and drying over irregular terrain. Advances in Water Resources 34(7):915–932,DOI 10.1016/j.advwatres.2011.04.017

Wang, Y., Liang, Q., Kesserwani, G., and Hall, J. W. (2011). "A positivity-preserving zero-inertia model for flood simulation." Comput. Fluids, 46(1), 505-511.

Yamazaki D., De Almeida G.a.M., Bates P.D. (2013) Improving computational efficiency in global river models by implementing the local inertial flow equation and a vector-based river network map. Water Resources Research 49(11):7221–7235, DOI 10.1002/wrcr.20552